The effect of barium on calcite $\{10\bar{1}4\}$ surfaces during growth

J. M. Astilleros,[1] C. M. Pina,[2,*] L. Fernández-Díaz,[1] and A. Putnis[2]

[1]Dpto. Cristalografía y Mineralogía, Universidad Complutense, 28040 Madrid, Spain
[2]Institut für Mineralogie, Universität Münster, Corrensstrasse 24, D-48149, Germany

Abstract—In situ atomic force microscopy (AFM) experiments have provided information about the effect of Ba^{2+} on crystal growth of calcite $\{10\bar{1}4\}$ surfaces. The microtopographic features observed have been interpreted by considering both the structural control that the calcite surfaces exert on the incorporation of divalent cations and the supersaturation state of the solution used. Pinning of the calcite growth steps occurs at low Ba concentrations, suggesting specific sites for Ba incorporation. When the Ba content of the solution is increased the advancement of monomolecular steps is observed. Although $[\bar{4}41]_+$ and $[48\bar{1}]_+$ steps advance showing characteristic jagged edges, the parallel steps (i.e., $[\bar{4}41]_-$ and $[48\bar{1}]_-$) remain practically immobile. This fact can be explained by considering the nonsymmetrically related distribution of large and small sites along the calcite steps and the easier incorporation of barium on the former. The measured increase in the height of the newly grown steps is also consistent with such preferential incorporation of Ba in certain positions. A further increase in the Ba concentration of the solutions leads to the formation of bidimensional nuclei on the calcite $\{10\bar{1}4\}$ surfaces. The nature of these nuclei is discussed taking into account the supersaturation of the solution with respect to two possible structures that can accommodate Ba: the calcite-type structure and the aragonite-type structure. *Copyright © 2000 Elsevier Science Ltd*

1. INTRODUCTION

The problem of incorporation of divalent cations during the precipitation of carbonates, and in particular during the crystallisation of calcite, has been extensively studied during the last two decades (Reddy and Nancollas, 1976; Morse, 1986; Falini et al., 1994). By determining cation/calcium distribution coefficients, paleowater compositions, climatic conditions, and diagenetic reactions involving carbonate solids have been frequently interpreted (Lorens, 1981; Mucci and Morse, 1983). In addition, the uptake of divalent metallic cations is directly related to important environmental and contamination problems (Davis et al., 1987; Zachara et al., 1991).

Whereas studies on the partitioning of some divalent cations, for example, Cd^{2+} (Lorens, 1981; Davis et al., 1987) and Sr^{2+} (Pingitore, 1986; Apitz, 1991), into calcite are relatively frequent, investigations into the partitioning of Ba^{2+} are more scarce. Numerous studies have demonstrated that there exists a direct relationship between the Ba content in sedimentary solid phases and biological activity in the oceans (Goldberg and Arrhenius, 1958; Chow and Goldberg, 1960; Bishop, 1988). Such a relationship is evidenced by a strong spatial and temporal correlation between the number of Ba-rich particles and higher organic carbon concentrations in seawaters (Dymond and Collier, 1996). It is clear that, to interpret with confidence the effect of biological processes on the Ba content in modern and ancient marine environments, a precise knowledge of the way in which Ba is removed from the water and how it is incorporated into crystalline solids is required. The most careful effort to study the thermodynamic aspects of incorporation of Ba^{2+} into the calcite was provided by Tesoriero and Pankow (1996). These researchers report a distribution coefficient for Ba^{2+} from an aqueous solution into calcite, $D_{Ba,eq}$, of 0.012 ± 0.005 and a miscibility limit, X_m, of 0.011. Such low values may reflect the inability of the calcite lattice to accommodate Ba^{2+} ions in calcium sites and is due to differences in their ionic radii (1 Å for Ca^{2+} and 1.34 Å for Ba^{2+}; Zachara et al., 1991) and their physicochemical properties, such as hydration, ionic mobility, electronegativity. On the other hand, the orthorhombic aragonite structure allows the uptake of higher amounts of Ba from aqueous solutions. However, under far-from-equilibrium conditions important deviations in the Ba/Ca distribution coefficients are observed and natural calcites with relatively high Ba contents have been found (Kitano et al., 1971; Hutcheon et al., 1985). The occurrence of natural and synthetic calcite, exhibiting phenomena such as compositional sectoral and intrasectoral Ba zoning (Paquette and Reeder, 1990, 1995), are good examples that indicate the existence of strong structural surface control. Moreover, the frequent alternation of aragonite and calcite containing different Ba/Ca ratios found in biominerals, such as marine shells, is evidence for the importance of the physicochemical conditions at a microscale on the carbonate crystallisation. It seems clear that the interrelation between external factors, namely the supersaturation with respect to the growing phase, and the surface structure determined by the crystallography and reactivity of the faces will play a decisive role in the Ba incorporation.

In this paper we present in situ atomic force microscope (AFM) observations of calcite $\{10\bar{1}4\}$ surfaces growing from Ba–Ca–CO_3 aqueous solutions. The microtopographic evolution of such surfaces indicates a clear structural control of the whole growth process: the presence of Ba in the solution strongly distorts the shape of the growth steps along certain crystallographic directions. In addition to such qualitative observations, the effect of the Ba concentration of the solutions on the growth kinetics has been evaluated measuring step velocities along nonequivalent crystallographic directions. To esti-

*Author to whom correspondence should be addressed (pina@nwz.uni-muesnter.de).

Table 1. Concentrations of the solutions used in the AFM growth experiments.

Experiment N°	[CaCl₂] (mmol/L)	[Na₂CO₃] (mmol/L)	[Ba(NO₃)₂] (mmol/L)	Ionic Strength
1	0.21	0.3	0.0	1.29×10^{-3}
2	0.24	0.3	0.4	2.53×10^{-3}
3	0.32	0.3	1.6	6.26×10^{-3}
4	0.46	0.3	4.0	1.37×10^{-2}

mate the departure from equilibrium of the crystallising system and to evaluate the possibility of formation of metastable phases, supersaturation calculations for the noncomplete $(Ba,Ca)CO_3$ solid solutions, considering both aragonite- and calcite-type structure, have been carried out. Our experimental results and calculations are consistent with both the microscopic theory of impurity incorporation (Sangwal, 1993, 1996) and models based on structural considerations (Reeder, 1996).

2. EXPERIMENTAL PROCEDURE AND SUPERSATURATION CALCULATIONS

Crystal growth experiments were carried out at 25°C in situ in a fluid cell of a Digital Instruments Multimode AFM working in contact mode. Calcite samples used as substrates were cleaved from a block of optically clear "Iceland Spar." Ca^{2+}–Ba^{2+}–CO_3^{-2} aqueous solutions were prepared by mixing Na_2CO_3, $Ba(NO_3)_2$ and $CaCl_2$ aqueous solutions (99+%). The pH of the solutions was measured using a TESTO 230 pH-meter. A value of 10.20 ± 0.05 was obtained in all cases. The pH-meter electrode (type 05 pH) was calibrated using 7.00 and 10.00 buffers (Shott Geräte). Table 1 shows the composition of the solutions used in the growth experiments. To avoid solution/sample equilibrium a flow of solution was maintained by injecting fresh solution at intervals of about 1 min between each AFM scan.

The supersaturation state of the solutions was evaluated considering that Ba can, to a limited extent, be incorporated into both rhombohedral (calcite) and orthorhombic (aragonite) structures. Therefore, the supersaturation will be not a single value, but a function of the solid composition as discussed by Prieto et al. (1993, 1997). The expressions used to calculate the supersaturations were:

$$\beta_{(Ba,Ca)CO_3}^{rhombohedral} = \frac{a(Ba^{2+})^x a(Ca^{2+})^{(1-x)} a(CO_3^{2-})}{(K_{BaCO_3,trig} a_{BaCO_3,trig})^x (K_{calcite} a_{calcite})^{(1-x)}} \quad (1)$$

$$\beta_{(Ba,Ca)CO_3}^{orthorhombic} = \frac{a(Ba^{2+})^x a(Ca^{2+})^{(1-x)} a(CO_3^{2-})}{(K_{witherite} a_{witherite})^x (K_{aragonite} a_{aragonite})^{(1-x)}} \quad (2)$$

where $a(Ca^{2+})$, $a(Ba^{2+})$, and $a(CO_3^{2-})$ are the activities of the free ions in the solution, and $K_{BaCO_3,rhomb} = 10^{-5.26}$, $K_{calcite} = 10^{-8.48}$, $K_{witherite} = 10^{-8.56}$, and $K_{aragonite} = 10^{-8.34}$ are the thermodynamic solubility products for the end-members of the solids solutions. The activity coefficients for Ca^{2+}, Ba^{2+}, and CO_3^{2-} were computed by using the extended Debye-Hückel formula (Stumm and Morgan, 1981). The aqueous speciation program used considered the following species: H^+, HCO_3^-, CO_3^{2-}, $NaCO_3^-$, Na^+, $Na_2CO_3^0$, $NaNO_3^0$, NO_3^-, $CaOH^+$, $CaHCO_3^+$, Ca^{2+}, OH^-, $H_2CO_3^0$, $NaHCO_3^0$, $NaOH^0$, $CaCO_3^0$, Ba^{2+}, $BaHCO_3^0$, $BaOH^+$, $BaCO_3^0$. Ion size parameters required to apply the extended Debye-Hückel formula were taken from Truesdel and Jones (1974). Table 1 (last column) shows the calculated ionic strength for the solutions. The ionic strength values ($I < 0.0137$) indicate that they are within the range of applicability of the extended Debye-Hückel formula. As an example of calculated solution compositions, Table 2 shows free ion and ion pair concentrations in experiment number 4. Note that the calculated pH value is very similar to our electrometric measurements. This is a test of the applicability of the speciation model used. The solubility products for calcite, aragonite, and witherite were taken from Plummer and Busenberg (1982) and Busenberg and Plummer (1986). The solubility product for $BaCO_3$ (rhombohedral) was calculated using the standard Gibbs free energy of formation given by

Table 2. Calculated free ion and ion pairs concentrations for the solution used in experiment number 4 (Table 1).

Free ions and ion pairs	Concentrations (mol/kg)	Free ions and ion pairs	Concentrations (mol/kg)
H^+	6.990×10^{-11}	$BaOH^+$	1.741×10^{-6}
OH^-	1.802×10^{-4}	$NaOH^0$	5.353×10^{-8}
Ca^{2+}	4.356×10^{-4}	$CaCO_3^0$	2.322×10^{-5}
Ba^{2+}	3.892×10^{-3}	$BaCO_3^0$	8.851×10^{-5}
NO_3^-	8.904×10^{-3}	$NaCO_3^-$	6.655×10^{-7}
Na^+	5.992×10^{-4}	$NaNO_3^0$	1.048×10^{-7}
CO_3^{2-}	9.471×10^{-5}	$CaHCO_3^+$	2.475×10^{-7}
HCO_3^-	9.048×10^{-5}	$BaHCO_3^+$	2.049×10^{-6}
$H_2CO_3^0$	1.145×10^{-8}	$NaHCO_3^0$	2.413×10^{-8}
$CaOH^+$	9.801×10^{-7}	$Na_2CO_3^0$	7.964×10^{-11}

Sverjensky and Molling (1992) and following the method proposed by Böttcher (1997).

Sverjensky and Molling (1992) calculate the standard Gibbs free energies of formation, at 25°C and 1 bar, of some crystalline solid phases that are often difficult or impossible to measure experimentally. They give an empirically linear free energy equation, applicable to cations of any charge, radius, and chemical type, which allows to estimate the free energies of solids, with an error lower than ± 4 kJ mol. They report on calculations for a number of hypothetical carbonates with the calcite structure, including $BaCO_3$. The solubility product of the hypothetical rhombohedral carbonates can be calculated from the expression:

$$\log K_{MeCO_3,rhomb} = (\Delta G_{f,MeCO_3,rhomb(s)}^0 - \Delta G_{f,Me^{2+}(aq)}^0 - \Delta G_{f,CO_3^{2-}(aq)}^0)/RT \ln 10 \quad (3)$$

where T is the temperature in degrees Kelvin, R is the gas constant (8.314 JK^{-1} mol^{-1}), and ΔG_f^0 are the standard Gibbs free energies of formation of the aqueous ions and the solid phase.

Substituting the standard free energies reported by Sverjensky and Molling (1992) and Berg and Vanderzee (1978) into Eqn. 3 for the case of the $BaCO_{3,rhomb}$ we obtain (calculations are summarised in Table 3): $K_{BaCO_3,rhomb} = 10^{-5.26}$.

Supersaturations, $\beta_{(Ba,Ca)CO_3}^{rhombohedral}$ and $\beta_{(Ba,Ca)CO_3}^{orthorhombic}$, were calculated for the solid phase composition intervals of $0 < X_{BaCO_3} < 0.1$ and $0.9 < X_{BaCO_3} < 1$. Within these intervals the solid solution was assumed to have ideal behaviour and the solid phase activities, $a_{BaCO_3,rhomb}$, $a_{calcite}$, $a_{witherite}$, and $a_{aragonite}$, were taken as equal to their molar fractions. This assumption is adequate here because changing the ideality of the solid phase does not change the form of the β functions, only their absolute value. For all the solutions used in the experiments the supersaturation with respect to the end-member calcite was $\beta = 5$.

3. RESULTS

At the start of each growth experiment, deionized water was passed over the crystal to clean the cleaved $\{10\bar{1}4\}$ calcite surfaces and to adjust the AFM parameters. This leads to a slight dissolution of cleavage steps and to the formation of etch pits. The etch pits on calcite usually show a typical rhombo-

Table 3. ΔG_f^0 values of ions (Ca^{2+}, Ba^{2+}, CO_3^{2-}) and rhomboedral Ca, Ba carbonates.

Ion	$\Delta G_{f,ion}^0$ (kJ/mol)	$\Delta G_{f,MeCO_3,rhomb}^0$ (kJ/mol)	$K_{MeCO_3,rhomb}$
Ca^{2+}	−552.79	−1129.18	$10^{-8.48}$
Ba^{2+}	−555.34	−1113.36	$10^{-5.26}$
CO_3^{2-}	−527.98	—	—

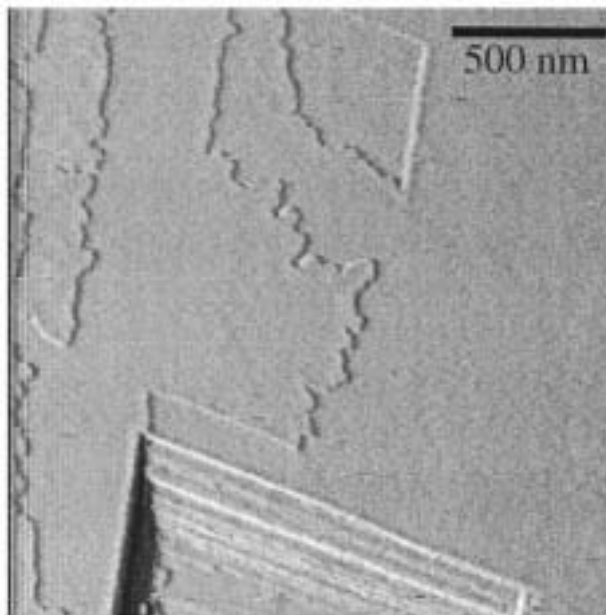Sverjensky and Molling 1992; Berg and Vanderzee, 1978.

Fig. 1 AFM image (taken in contact mode and displaying deflection signal, which enhances the contrast between topographic features) showing the development of lobes near to an etch pit from initially straight [$\bar{4}$41] steps. The distance between lobes is approximately 80 nm

Fig. 2 Growing calcite {10$\bar{1}$4} surface in a supersaturated solution with respect to calcite ($\beta_{cal} = 5$) and [Ba] = 1.6 mmol/L. (a) AFM image was taken in constant force mode while displaying the cantilever deflection signal. The advance of jagged monomolecular [$\bar{4}$41]$_+$, [48$\bar{1}$]$_+$, and [010]$_+$ steps with a height of ~3 Å can be observed. The distance between lobes is around 40 nm. Note the different contrast of the newly grown steps edges. (b) Height AFM image of the same area as (a). The brighter step edges indicate that the newly grown steps are slightly thicker than the initial ones

hedral shape defined by the [$\bar{4}$41] and [48$\bar{1}$] steps. Because these two pairs of steps are not crystallographically equivalent they dissolve with different velocities. Two fast steps, [$\bar{4}$41]$_+$ and [48$\bar{1}$]$_+$, and two slow steps, [$\bar{4}$41]$_-$ and [48$\bar{1}$]$_-$, can be distinguished (Hillner et al., 1992). Therefore, by direct observation of the development of such etch pits it was possible to determine unequivocally the crystallographic directions on calcite {10$\bar{1}$4} surfaces before each growth experiment.

Once the directions on the calcite substrate are known, Ca^{2+}–Ba^{2+}–CO_3^{-2} solutions with the concentrations shown in Table 1 were injected into the fluid cell of the AFM. In all the experiments, growth on the surface is observed and a few minutes after injecting the solutions, the growing step edges become jagged or dendritic. This is a general microtopographic feature observed on the calcite surfaces whenever barium is present in solution. Figure 1 shows details of such dendritic growth on a calcite {10$\bar{1}$4} surface from a solution with [Ba] = 0.4 mmol/L. In this image rounded dendrites develop from initially straight [$\bar{4}$41] steps. Observations made on a number of images indicate that the degree of roughness of jagged and dendritic steps is related to the Ba concentration of the solution. Thus, lower concentrations of Ba result in dendrites with larger distances between the reentrants of the lobes, whereas at higher Ba concentrations the steps exhibit fine jagged saw-like edges. For a Ba concentration of 0.4 mmol/L the average distance between lobules is 80 um and for a Ba concentration of 1.6 mmol/L it is reduced to 40 nm. The formation of irregular step fronts correlates with the slowing of step rates. Initially, the growth steps advance relatively fast and their velocity progressively decreases until a steady value, which depends on the Ba concentration, is reached. The time elapsed from the beginning of each experiment to this new growth regime decreases with
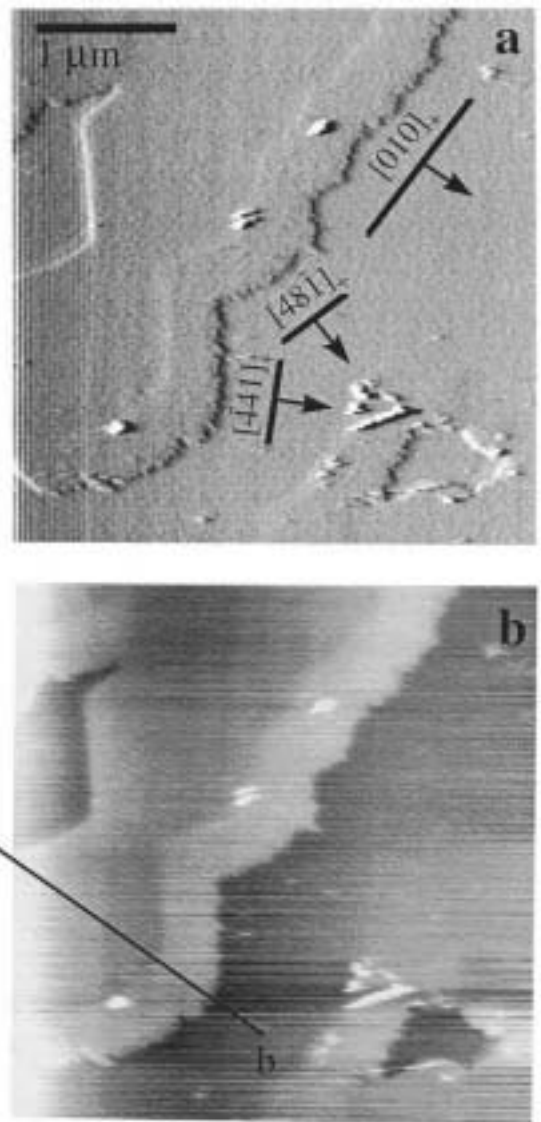
increasing Ba in the solution. Figure 2 shows a representative example of the growth behavionr on a calcite {10$\bar{1}$4} surface from a Ba-rich solution moderately supersaturated with respect to calcite ($\beta = 5$). This AFM image was taken 650 s after growth began. Although [$\bar{4}$41]$_+$ and [48$\bar{1}$]$_+$ monomolecular steps advance showing the typical jagged edges, the parallel ones (i.e., [$\bar{4}$41]$_-$ and [48$\bar{1}$]$_-$) remain practically immobile. The advancement of steps parallel to [010] and toward the plus direction is also observed. Another interesting microtopographic feature observed in the AFM images is that the [$\bar{4}$41]$_+$, [48$\bar{1}$]$_+$, and [010]$_+$ step edges contrast with the rest of the
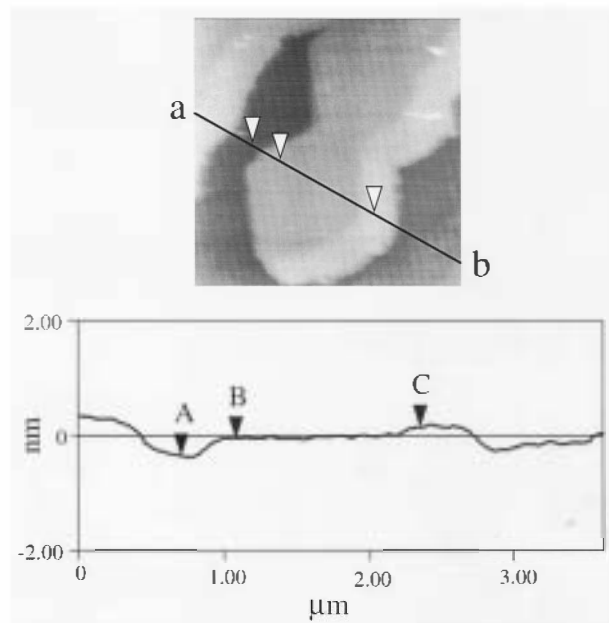
Fig. 3. (a) Detail of newly grown steps shown in Fig. 2b. (b) Height profile along line a–b. The height between points A and B is 3.02 Å, the thickness of an elementary calcite ($10\bar{1}4$) growth layer. The measured height between points A and C is 4.6 Å.

scanned area after some time of growth (Fig. 2a). This is more evident in the height image of the same area shown in Figure 2b, where the brighter areas correspond to the newly grown edges, indicating that they are higher than the initial steps. In Figure 3 details of the growing steps shown in Figure 2 can be observed. Height measurements made along the a–b transect give a value of ~3.0 Å for the initial steps, i.e., the thickness of the elementary calcite growth layer, and a height of ~4.6 Å for the newly grown step edges. The precision of the height measurements is about ±0.2 Å.

The presence of barium in the solutions not only affects the shape of the growth steps, but also the step velocities for the equivalent $[\bar{4}41]_+$ and $[48\bar{1}]_+$ steps and for the $[010]_+$ step. In Figure 4 the rate of the advancement of the fast steps ($[\bar{4}41]_+$, $[48\bar{1}]_+$, and $[010]_+$) was plotted for solutions with different Ba concentrations, and a supersaturation with respect to pure calcite of $\beta = 5$. In all cases step advancement is linear with time once the transient dendritic state is overcome. Step velocities calculated from the slope of the fitted lines are shown in Figure 5. For Ba-free solutions the growth rate of the fast steps (i.e., pure calcite) is 2.66 nm/s. The presence of a small amount of Ba in the solution ([Ba] = 0.4 mmol/L) results in a strong reduction of the step rate to values around to 0.2 nm/s. However, a further increase of the Ba content of the solutions leads to a progressive increase in the step velocities until for Ba concentrations above 2.5 mmol/L the steps velocities reach a constant value ~1.3 nm/s. The dependence of the step rate on the Ba concentration is shown in Figure 5.

For a Ba concentration of [Ba] = 4 mmol/L, in addition to the step advancement, a subsequent two-dimensional nucleation event occurs. Two-dimensional nuclei are ~4.4 Å in height and are preferentially formed on the previously grown steps. Only a few of them appear on the original surface. Figure
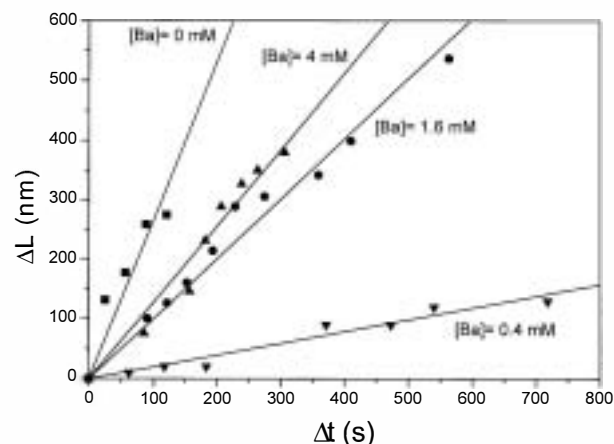

Fig. 4. Step advancement for $[\bar{4}41]_+$, $[48\bar{1}]_+$, and $[010]_+$ steps versus time from solutions with different concentrations of barium.

6 shows a calcite $\{10\bar{1}4\}$ surface on which step advancement and two-dimensional nucleation can be observed. Nuclei grown on the new steps do not show crystallographic forms and are elongated with the longer axis approximately parallel to the $[48\bar{1}]$ direction. They also exhibit a high nucleation density (~45 nuclei/μm^2) in comparison to the scarcer, bigger, and polygonized nuclei grown on the $\{10\bar{1}4\}$ terraces (~5 nuclei/μm^2). In some regions of the surface the small nuclei coalesce and form aggregates.

4. DISCUSSION

The AFM observations presented in the previous section clearly reveal the interrelation between the calcite $\{10\bar{1}4\}$ surface structure and the presence of Ba in the solution from which such a surface is growing. The most evident microtopographic features derived from this interrelation are the strong anisotropy of the step growth, the development of jagged or dendritic step edges, and the increase of the step thickness. To explain these observations we first consider in detail the nature
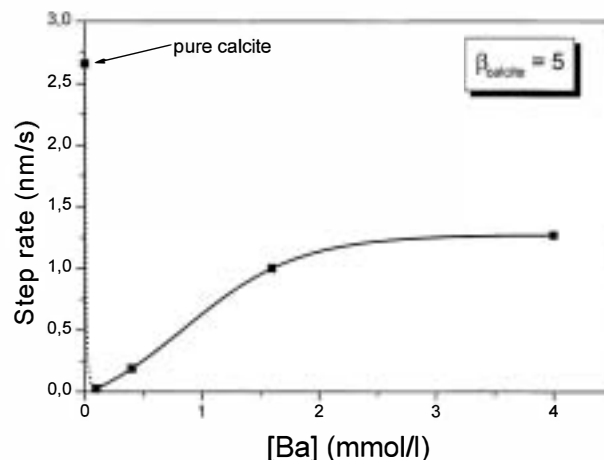

Fig. 5. Velocity of the fast steps in calcite vs. Ba concentration in solution. The supersaturation with respect to calcite was maintained constant at $\beta = 5$ in all cases.
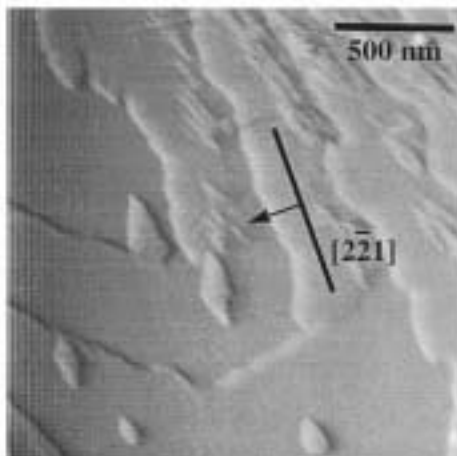
Fig. 6 Growing calcite $\{10\bar{1}4\}$ surface in a supersaturated solution with respect to calcite ($\beta_{cal} = 5$) and [Ba] = 4 mmol/L. The image was taken in constant force mode while displaying the cantilever deflection signal. The advancement of the $[2\bar{2}1]_+$ thick step and the formation of two-dimensional nuclei on the surface and preferentially on the newly grown steps can be seen

of the $\{10\bar{1}4\}$ calcite surfaces. The $\{10\bar{1}4\}$ faces, which define the calcite cleavage rhombohedron, contain three nonequivalent periodic bond chains (PBCs) parallel to the $\langle 441 \rangle$, $\langle 2\bar{2}1 \rangle$, and $\langle 010 \rangle$ directions and, therefore, are flat (F) faces (Heijnen, 1985). Steps parallel to a given set of PBCs are structurally identical but, because of the orientation of such steps to the symmetry elements, opposite senses of advancement for a given step are not equivalent ($[\bar{4}41]_+$, $[48\bar{1}]_+$, and ($[\bar{4}41]_-$, $[48\bar{1}]_-$ according to the notation used by Staudt et al., 1994). Experimentally determined growth and dissolution rates show that positive steps migrate faster than negative steps (Hillner et al., 1992). Furthermore, this nonequivalence of growth steps is considered by Paquette and Reeder (1990, 1995) and Staudt et al. (1994) as the main reason for the differential incorporation of the trace elements into the calcite structure. In the model proposed by these investigators two general types of kinks along $\langle 441 \rangle$ steps can be distinguished: the less constrained and larger sites, distributed along $[\bar{4}41]_+$, $[48\bar{1}]_+$ steps, and the more constrained and smaller ones, which are present in the $[\bar{4}41]_-$, $[48\bar{1}]_-$ steps. Larger cations than Ca (Ba and Sr, for example) tend to incorporate in positive steps, whereas cations smaller than Ca (Mn, Mg, Co, Cd) will be preferentially incorporated in negative steps.

To understand the way in which different cations are incorporated into the calcite $\{10\bar{1}4\}$ F faces it is also necessary to consider the influence of impurity adsorption on the crystal growth behaviour. The influence of impurity adsorption on the velocity of movement of steps on the crystal surface can be explained by the microscopic theory of impurity incorporation. According to Sangwal (1993, 1996) the impurity adsorption behaviour critically depends on both the impurity concentration and the available sites on the surface. The number of available sites, n_{ava}, on F surfaces of a crystal showing the same microtopographic features (i.e., step density and kink density) is constant. In contrast, the number of sites occupied by the impurity, n_{occ}, depends on their concentration. The ratio $\theta = n_{occ}/n_{ava}$ gives the degree of coverage of the adsorption sites on

the surface. When the impurity concentration is very low, i.e., $\theta \ll 1$, their adsorption at specific sites leads to the pinning of the step edges and, therefore, a reduction of the velocity of advancement. This has been recently shown by Teng et al. (1999) for calcite growth in the presence of trace amounts of divalent cations. In this regime an increase of impurity concentration results in a further slowing of the step rate. With increasing impurity concentration in the growth medium, θ can be higher than unity and the excess of impurities may produce clusters or precipitates on the crystal surface. In such a situation the formation of an epitaxial layer with structural similarities to the original surface is possible.

It is clear that the different impurity incorporation behaviour described above will strongly depend on the supersaturation state of the solution with respect to the possible solids forming on the surface. In the system Ba-Ca-CO$_3$–H$_2$O both calcite- and aragonite-type structures can accommodate Ba, although the solid solutions are very restricted: CaCO$_3$ (calcite) can only accommodate small amounts of Ba, whereas BaCO$_3$ (aragonite structure) can accommodate only small amounts of Ca. Supersaturation calculations presented here were carried out assuming that: (1) the solid solutions (Ca,Ba)CO$_3$ (rhombohedral) and (Ba,Ca)CO$_3$ (orthorhombic) behave ideally in the proximity of the end-member compositions and (2) there exists a theoretical BaCO$_3$ end-member with calcite structure whose thermodynamic properties (and in particular its solubility product) can be empirically derived from its Gibbs free energy of formation and coordination schemes (Sverjensky and Molling, 1992; Böttcher, 1997).

Figure 7 shows the calculated supersaturations, $\beta_{(Ba,Ca)CO_3}^{rhombohedral}$ and $\beta_{(Ba,Ca)CO_3}^{rhombohedral}$, for the solutions used in the experiments (Table 1) in the compositional ranges $0 < X_{BaCO_3} < 0.1$ and $0.9 < X_{BaCO_3} < 1$. As can be seen, higher Ba concentrations of the solutions result in higher supersaturation with respect to both the calcite and aragonite structures. For Ca-rich solids, supersaturation is not strongly dependent on the solid structure. As a consequence, similar supersaturation values with respect to both calcite and aragonite structures were obtained. Conversely, when very Ba-rich solids are considered, the supersaturation for the aragonite structure is higher than the supersaturation for the calcite structure. Our calculations clearly suggest that the formation of a Ba-rich solid solution (Ba,Ca)CO$_3$ (orthorhombic) is favoured.

AFM observations show that the $[\bar{4}41]_+$, $[48\bar{1}]_+$, and $[010]_+$ steps growing from Ca–Ba-CO$_3$ solutions are always the faster ones, in agreement with the anisotropic growth behaviour reported for pure calcite (Hillner et al., 1992; Gratz et al., 1993). This is also consistent with the model of selective incorporation of large and small cations on $\{10\bar{1}4\}$ calcite surfaces proposed by Paquette and Reeder (1995). In addition, the microtopographic features observed in our AFM experiments agree with the general model of impurity incorporation described above and allow us to explain the kinetic data obtained. When the concentration of barium in the solution is low (e.g., [Ba] = 0.4 mmol/L) the step velocity is substantially modified because Ba^{2+} cations adsorb onto specific sites along the steps and pin them. Such pinning of steps results in a strong reduction of the step rate in comparison to pure calcite (dashed line in Fig. 5). For solutions containing higher amounts of barium (i.e., [Ba] = 1.6 mmol/L and [Ba] = 4 mmol/L) the pinning of steps is a

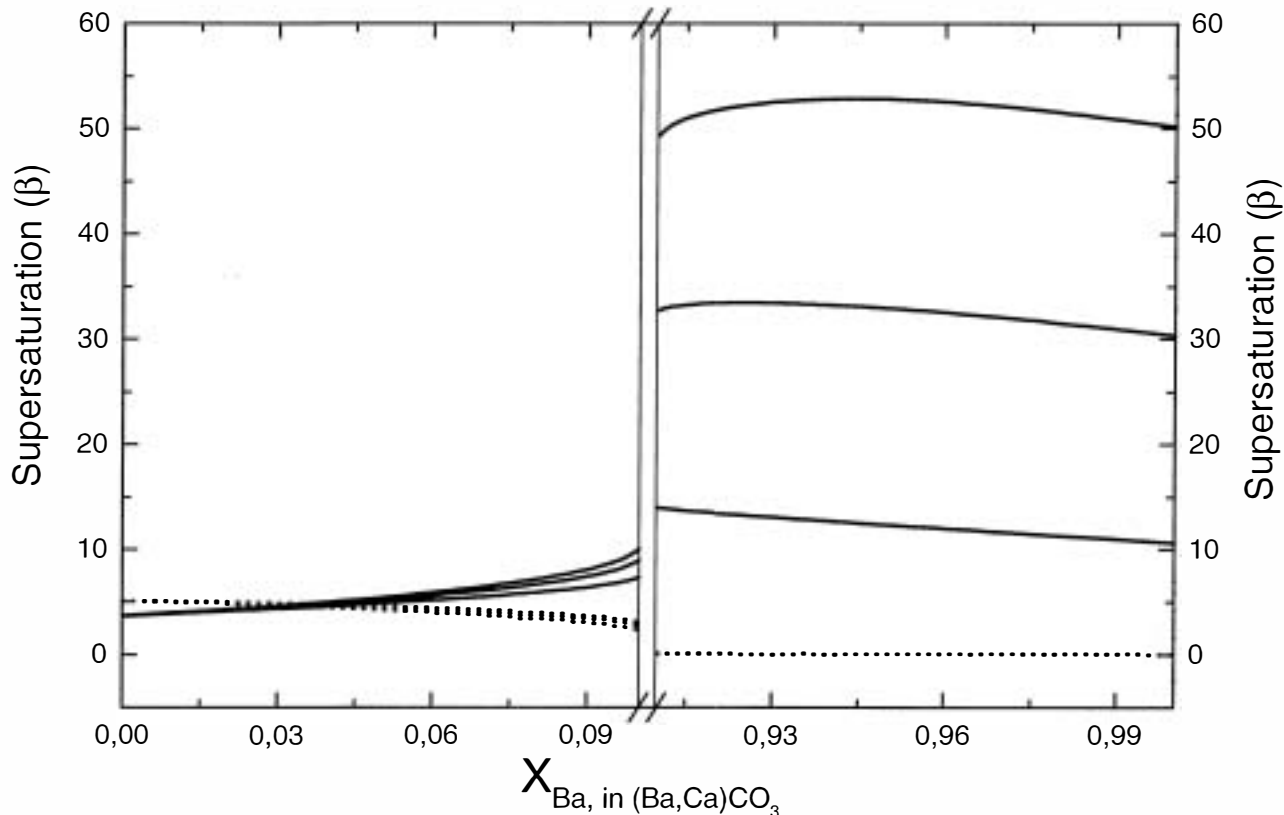Fig. 7. Supersaturation curves calculated for solutions with compositions: [Ba] = 0.4 mmol/L, [Ba] = 1.66 mmol/L, and [Ba] = 4 mmol/L and constant supersaturation for calcite in the compositional ranges of the solid $0 < X_{BaCO_3} < 0.1$ and $0.9 < X_{BaCO_3} < 1$. Solid curves correspond to the aragonite-type structure and dotted curves to the calcite-type structure. Increasing Ba contents in the aqueous solutions result in higher supersaturations with respect to the aragonite phase. In contrast, the calcite phase shows low and quite constant supersaturation.

transient state. Therefore, once the saturation of adsorption sites occurs, and all available sites are occupied, steps start to grow according to a different mechanism and the step migration is accelerated. In this new regime the step velocity is directly related to the Ba concentration. However, the value of ~1.3 nm/s, reached for the maximum concentration of barium used, seems to be a maximum step velocity value, indicating a steady-state regime for a further increase of Ba concentrations. These steps clearly exhibit a higher thickness than the "normal" calcite steps (~1.6 Å higher). When a Ba concentration of [Ba] = 4 mmol/L was used heterogeneous nucleation on the surface is observed.

At this point a question arises: What is the nature of both steps and nuclei? Our measurements on both steps and nuclei indicate a higher thickness than that expected for Ba incorporation only in the Ca crystallographic sites in calcite. Furthermore, as mentioned above, the supersaturation of the solutions used in this work with respect to an aragonite-type structure containing Ba is much higher than for a calcite-type structure (and for very high Ba concentrations the supersaturation should be enough to promote homogeneous nucleation of a Ba-rich phase with the aragonite structure). A possible interpretation is the heterogeneous nucleation of an orthorhombic (Ba,Ca)CO$_3$ solid on the calcite surface, preferentially in continuity with step edges. This nucleation can be also favoured by the simi-

larities of calcite- and aragonite-type structures (Rao and Rao, 1978). If we consider, for example, the (110) planes in the aragonite structure, which are, morphologically, the most important, we find an interplanar spacing of 4.21 Å for pure aragonite and 4.56 Å for pure witherite. The measured height of both steps and nuclei (4.5 Å) is in agreement with this range of thickness and it would suggest a solid with composition close to witherite. Other planes, such as (020) or (111) of the aragonite structure, also have similar interplanar spacing to calcite $\{10\bar{1}4\}$ plane spacing and, in principle, they could also be epitaxial planes. In addition, the fact that the step velocities measured for the thick steps are always lower than for the calcite (although the supersaturations are quite high) seems also to support the idea of an epitaxial growth of an orthorhombic carbonate on a substrate of calcite, which cannot grow as fast as pure calcite.

Another alternative explanation for the nature of the thick steps would be that such steps are calcite steps growing in continuity with the preexisting substrate and incorporating Ba in nonlattices sites (Pingitore, 1986). Then, the higher step thickness might be explained as the consequence of an anomalous deformation of the $\{10\bar{1}4\}$ planes (unrelated to the substitution of Ca^{2+} positions by Ba^{2+}). In such a case, the newly formed steps would be highly metastable and more soluble than the "normal" calcite steps.

Finally, a number of natural double calcium barium carbonates, which exhibit similar orthorombic structures (e.g., barytocalcite, alstonite and paralstonite), are also phases that could form in continuity with the original steps (Speer, 1983). However, because of the lack of information about the physicochemical properties of barium calcium carbonates, and the fact that the AFM technique gives no information on either the chemistry or crystallography of the crystal surfaces, the complete determination of the processes occurring on growing calcite surfaces is not possible at the moment. Moreover, the justification of the suggested epitaxial growth requires a detailed study of the structures involved, and their crystallographic and surface energy relationships, which is beyond the scope of this work. Nevertheless, AFM observations demonstrate that the calcite surface structure not only controls the incorporation of cations during its growth, but it also exerts a strong influence when the supersaturation conditions of the solution allow the formation of other solid phases. The nucleation and growth of such phases at a nanometer scale on calcite surfaces may be related to some observed anomalies in natural carbonate Ba/Ca distribution coefficients.

REFERENCES

Apitz S. E. (1991) The lithification of ridge flank basal carbonates: Characterisation and implications for Sr/Ca and Mg/Ca in marine chalks and limestones. Ph.D. dissertation, Univ. California.

Berg L. B. and Vanderzee C. E. (1978) Thermodynamics of carbon dioxide and carbonic acid: (a) the standard enthalpies of solution of $Na_2CO_3(s)$, $NaHCO_3(s)$, and $CO_2(g)$ in water at 298.15 K; (b) the standard enthalpies of formation, standard Gibbs energies of formation, and standard entropies of $CO_2(aq)$, $HCO_3^-(aq)$, $CO_3^{2-}(aq)$, $NHCO_3(s)$, $Na_2CO_3(s)$, $Na_2CO_3.H_2O(s)$, and $Na_2CO_3.10H_2O(s)$. *J. Chem. Thermodynamics* **10**, 1113–1136.

Bishop J. K. B. (1988) The barite–opal–organic carbon association in oceanic particulate matter. *Nature* **331**, 341–343.

Böttcher M. E. (1997) Comment on solid solution partitioning of Sr^{2+} Ba^{2+} and Cd^{2+} to calcite, by A. J. Tesonaro and J. F. Pancow. *Geochim. Cosmochim. Acta* **61**, 661–662.

Busenberg E. and Plummer L. N. (1986) The solubility of $BaCO_3$ (witherite) in CO_2–H_2O solutions between 0 and 90°C, an evaluation of the association constants of $BaHCO_3^+(aq)$ and $BaCO_3^0(aq)$ between 5 and 80°C, and preliminary evaluation of the thermodynamic properties of Ba^{2+}. *Geochim. Cosmochim. Acta* **50**, 2225–2233.

Chernov A. A. (1984) *Modern Crystallography III: Crystal Growth.* Springer series in Solid-State Sciences. Vol. 36, Chap. 4. Springer-Verlag.

Chow T. J. and Goldberg E. D. (1960) On the marine geochemistry of barium. *Geochim. Cosmochim. Acta* **20**, 192–198.

Davis J. A., Fuller C. C., and Cook A. D. (1987) A model for trace metal sorption processes at the calcite surface: adsorption of Cd^{2+} and subsequent solid solution formation. *Geochim. Cosmochim. Acta* **51**, 1477–1490.

Dymond J. and Collier R. (1996) Particulate barium fluxes and their relationships to biological productivity. *Deep-Sea Research II* **43**, 1283–1308.

Falini G., Gazzano M., and Ripamonti A. (1994) Crystallization of calcium carbonate in presence of magnesium and polyelectrolytes. *J. Crystal Growth* **137**, 577–584.

Goldberg E. and Arrhenius G. O. S. (1958) Chemistry of pacific sediments. *Geochim. Cosmochim. Acta* **13**, 153–212.

Gratz A. J., Hillner P. E., and Hansma P. K. (1993) Step dynamics and spiral growth on calcite. *Geochim. Cosmochim. Acta* **57**, 491–495.

Heijnen W. M. M. (1985) The morphology of gel grown calcite. *N. Jb. Miner. Mh.* **8**, 357–381.

Hillner P. E., Gratz A. J., Manne S., and Hansma P. K. (1992) Atomic scale imaging of calcite growth and dissolution in real time. *Geology* **20**, 359–362.

Hutcheon I., Nahnybida C., and Krouse H. R. (1985) The geochemistry of carbonate cements in the Avalon Sand, Grand Banks of Neufoundland. *Mineralogical Mag.* **49**, 457–467.

Kitano Y., Kanamori N., and Oomori T. (1971) Measurements of distribution coefficients of strontium and barium between carbonate precipitate and solution-abnormally high values of distribution coefficients measured at early stages of carbonate formation. *Geochem. J.* **4**, 183–206.

Lorens R. B. (1981) Sr, Cd, Mn, and Co distribution coefficients in calcite as a function of calcite precipitation rate. *Geochim. Cosmochim. Acta* **45**, 553–561.

Morse J. W. (1986) The surface chemistry of calcium carbonate minerals in natural waters: An overview. *Mar. Chem.* **20**, 91–112.

Mucci A. and Morse J. W. (1983) The incorporation of Mg^{2+} and Sr^{2+} into calcite overgrowths. *Geochim. Cosmochim. Acta* **47**, 217–233.

Paquette J. and Reeder R. J. (1990) New type of compositional zoning in calcite: Insights into crystal growth mechanisms. *Geology* **18**, 1244–1247.

Paquette J. and Reeder R. J. (1995) Relationship between surface structure, growth mechanism, and trace element incorporation in calcite. *Geochim. Cosmochim. Acta* **59**, 735–749.

Pingitore N. E., Jr. (1986) Modes of cooprecipitation of Ba^{2+} and Sr^{2+} with calcite. In *Geochemical Processes at Mineral Surfaces* (ed. J. A. Davis and K. F. Hayes), pp. 574–586. ACS Symp. Ser. 323.

Plummer L. N. and Busenberg E. (1982) The solubilities of calcite, aragonite and vaterite in CO_2–H_2O solutions between 0 and 90°C, and an evaluation of aqueous model for the system $CaCO_3$–CO_2–H_2O. *Geochim. Cosmochim. Acta* **46**, 1011–1040.

Prieto M., Putnis A., and Fernández-Díaz L. (1993) Crystallization of solid solutions from aqueous solutions in a porous medium: Zoning in $(Ba,Sr)SO_4$. *Geol. Mag.* **130**, 289–299.

Prieto M., Fernández-González A., Putnis A., and Fernández-Díaz L. (1997) Nucleation, growth and zoning phenomena in crystallizing $(Ba,Sr)CO_3$, $Ba(SO_4, CrO_4)$, $(Ba,Sr)SO_4$, and $(Cd, Ca)CO_3$ solid solutions from aqueous solutions. *Geochim. Cosmochim. Acta* **61**, 3383–3397.

Rao C. N. and Rao K. J. (1978) *Phase Transitions in Solids.* McGraw-Hill.

Reddy M. M. and Nancollas G. H. (1976) The crystallization of calcium carbonate. IV. The effect of magnesium, strontium and sulfate ions. *J. Crystal Growth* **35**, 33–38.

Reeder R. J. (1996) Interaction of divalent cobalt, zinc, cadmium, and barium with the calcite surface during layer growth. *Geochim. Cosmochim. Acta* **60**, 1543–1552.

Sangwal K. (1993) Effect of impurities on the processes of crystal growth. *J. Crystal Growth* **128**, 1236–1244.

Sangwal K. (1996) Effects of impurities on crystal growth processes. *Prog. Cryst. Growth and Charact.* **32**, 3–43.

Speer J. A. (1983) Crystal chemistry and phase relations of orthorombic carbonates. In *Carbonates: Mineralogy and Chemistry. Reviews in Mineral.* Vol. 11, 145–190. *Min. Soc. America.*

Staudt W. J., Reeder R. J., and Schoonen M. A. A. (1994) Surface structural controls on compositional zoning of SO_4^{2-} and SeO_4^{2-} in synthetic calcite single crystals. *Geochim. Cosmochim. Acta* **58**, 2087–2098.

Stumm W. and Morgan J. J. (1981) *Aquatic Chemistry. An Introduction Emphasizing Chemical Equilibria in Natural Waters.* Wiley-Interscience.

Sverjenski D. A. and Molling P. A. (1992) A linear free energy relationship for crystalline solids and aqueous ions. *Nature* **356**, 231–234.

Teng H. H., Dove P. M., and DeYoreo J. J. (1999) Reversed calcite morphologies induced by microscopic growth kinetics: Insight into biomineralization. *Geochim. Cosmochim. Acta* **58**, 2087–2098.

Tesoriero A. J. and Pankow J. F. (1996) Solid solution partitioning of Sr^{2+}, Ba^{2+}, and Cd^{2+} to calcite. *Geochim. Cosmochim. Acta* **60**, 1053–1063.

Truesdel H. A. and Jones B. F. (1974). WATEQ, a computer program for calculating chemical equilibria of natural waters. U.S. Geological Survey. *J. Res.* **2**, 233–248.

Zachara J. M., Cowan C. E., and Resch C. T. (1991) Sorption of divalent metals on calcite. *Geochim. Cosmochim. Acta* **55**, 1549–1562.